Analytical Models of Degassing and Regassing Geothermal Systems

David Dempsey[1]

[1]University of Canterbury

david.dempsey@canterbury.ac.nz

Keywords: *Carbon dioxide, emissions, lumped parameter model, depressurisation, analytical solution, degassing.*

ABSTRACT

Geothermal systems naturally contain dissolved carbon dioxide, which may be present in the liquid reservoir at concentrations up to saturation. Observations from several geothermal systems have identified a degassing trend over time associated with production. More recently, attention has turned to the reinjection of CO_2 into the reservoir or adjacent aquifers.

The dynamics of CO_2 in a geothermal reservoir are influenced by several physical processes. Changes in pressure and temperature can reduce solubility in the liquid phase and may lead to exsolution if concentration is already close to saturation. CO_2 may escape the reservoir by migrating vertically through pathways in the caprock or via lateral outflow. CO_2 can be directly extracted from the reservoir through wells and may in some cases be partially or fully returned through reinjection. Finally, CO_2 can participate in geochemical reactions with the host rock.

Given the potential for complex physical interactions, numerical reservoir modelling is often the preferred method for characterising the state and trajectory of a given geothermal system. However, under certain simplifications a set of closed-form analytical solutions can be developed. This study describes a lumped parameter ODE model of a liquid geothermal reservoir subject to pressure decline, degassing, production-reinjection and mineralisation.

Solutions are developed for a high-gas system where CO_2 concentration is solubility limited, and a low-gas system that hosts negative emissions (carbon removal) and mineralisation. The high-gas system undergoes an early period of degassing as pressure declines and then reaches a new equilibrium where net total emissions exceed the pre-production baseline due to an induced upflow effect. The low gas system with additional CO_2 reinjection is only able to achieve negative emissions over the long-term when mineralisation is present.

1. INTRODUCTION

1.1 Geothermal CO_2 emissions

Natural and anthropogenic CO_2 fluxes (i.e., power plant emissions) associated with geothermal systems are receiving increased attention in the context of national emissions reduction. An accurate accounting of geothermal emissions is important for the geothermal industry to receive fair treatment under emissions pricing schemes. In particular, consideration should be given to the natural propensity of geothermal systems to flux CO_2, even in the absence of power production. Furthermore, these natural fluxes may be disturbed, and potentially reduced, by power production. This effect might be deducted from the obligations of the developer (Bertani and Thain, 2002; O'Sullivan et al., 2021).

In New Zealand, 21 out of 22 high-temperature geothermal systems locate in the Taupo Volcanic Zone of the central North Island (Bibby et al., 1995) with only the Ngāwhā field in Northland located outside this region. Geochemical analysis of these systems (Seward and Kerrick, 1996) reveals a range of CO_2 content in the liquid reservoir, from 0.04 to 2.2 weight percent. Isotopic analysis (Giggenbach, 1995) indicates this CO_2 is magmatically derived and total natural emissions through NZ geothermal systems are estimated to exceed 400 $kt.yr^{-1}$ (Seward and Kerrick, 1996). In comparison, in 2017 CO_2 emissions from twelve NZ power stations totalled 600 $kt.yr^{-1}$, although this number has been declining due to changes in reservoirs and the increasing adoption of gas reinjection (Mclean et al., 2024).

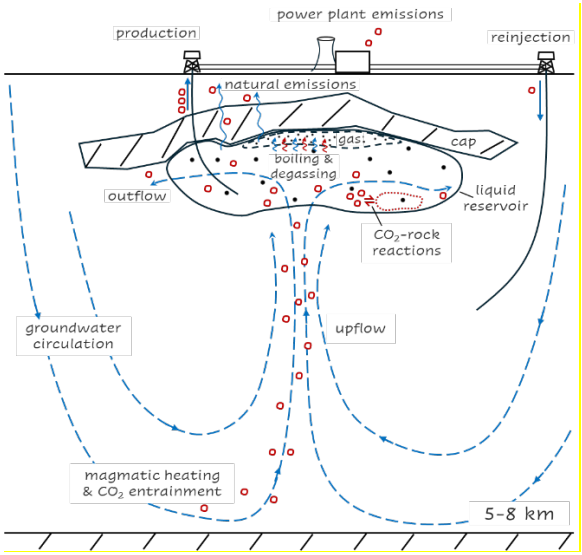

Figure 1: Conceptual model of CO_2 flux and key groundwater processes through a produced geothermal system.

The CO_2 flux dynamics of a geothermal reservoir is influenced by numerous physical processes (Fig. 1). First, CO_2 dissolved in the liquid phase can be transported in and out of the reservoir by associated pressure driven upflow and outflow (lateral and vertical), which may be disturbed from its natural equilibrium by production and reinjection. Second, CO_2 is extracted from the reservoir alongside the produced fluid either as a minor component present in the liquid phase or a potentially major constituent of the gas-phase. Preferential partitioning leads to high CO_2 concentrations in the gas phase (Grant, 1977; O'Sullivan et al., 1983) and the early-time phenomenon of "degassing" where this component is quickly stripped from the reservoir. Some fraction of the produced CO_2 may be captured and reinjected into the geothermal system, potentially alongside other CO_2 sources (e.g., Titus et al., 2025). Third, and related to the previous, are the effects of depressurisation (either through production or upflow) that decreases the maximum

Proceedings 47th New Zealand Geothermal Workshop
11 -13 November 2025
Rotorua, New Zealand
ISSN 2703-4275

solubility of CO_2 in the liquid and may induce a wider degassing than CO_2 stripping from the gas cap. Finally, dissolved CO_2 can react with certain rock types that might be present in the reservoir, with basaltic components in Iceland a notable example (Snaebjörnsdóttir et al., 2020).

1.2 Prior modelling of CO_2 in geothermal systems

Early modelling studies of CO_2-rich geothermal fields focused on role of the CO_2 component in shifting the thermodynamic behaviour of the reservoir. At Ohaaki, a high concentration of CO_2 causes boiling to 2 km depth in the natural state. Both lumped parameter (tank) (Grant, 1977) and column models (O'Sullivan et al., 1985) emphasised the rapid initial pressure drop from CO_2 escaping the bores ("degassing") and the role of relatively permeability.

Subsequent models of Ohaaki have progressed towards higher spatial and temporal resolution (O'Sullivan et al., 2021; O'Sullivan et al., 2025), with a focus on improved geological modelling and history matching. As a result, O'Sullivan et al. (2021) suggest the natural state CO_2 flux at Ohaaki to be approximately 140 kt.yr^{-1} substantially higher than the 30 kt.yr^{-1} estimated by Seward and Kerrick (1996). They further resolve discrete episodes of degassing associated with early production testing, a steady decline in natural state emissions as the field is produced, and a multi-decade recovery to steady state after closure. The decline in natural state emissions during production highlights the value of a holistic understanding of the field for emissions accounting. A feature of the O'Sullivan et al. (2021) model is that CO_2 mass input at the base of the model occurs at a fixed rate.

Recent modelling studies have turned towards the role of CO_2 reinjection in geothermal fields. Kaya and Zarrouk (2017) modelled reinjection of CO_2 and other gases into a generic geothermal reservoir and showed that a variety of impacts on the production are possible depending on injection strategy. Swanepoel et al. (2024) extended this to include injection of additional CO_2 beyond that captured from the field for negative emissions applications. They found a steady increase in CO_2 returning to the production wells. Recent advances have also included coupled reactions between dissolved CO_2 and reservoir minerals (Siahaan et al., 2024.

The models developed in this study are a deliberate de-evolution from modern reservoir simulations that capably replicate field dynamics at high resolution. Through reanimation of the lumped parameter framework described by Fradkin et al, (1981), we step back to a simpler, system-level view. These models are inadequate to match and predict trajectories of individual systems, but they do nevertheless allow us to identify the relevant characteristic time scales of CO_2 fluxing geothermal systems, and how these govern the response to future production.

2. METHODOLOGY

This study develops analytical expressions to describe changes in CO_2 concentration and flux from a geothermal reservoir. It builds on a number of standard (if idealized) concepts that are introduced here.

The reservoir comprises a cylindrical region of porous rock with surface area S [m^2], height H [m], volume $V = SH$ [m^3], and porosity ϕ [-]. Mass and pressure changes are such that V, ϕ and density ρ [kg.m^{-3}] are treated as constant.

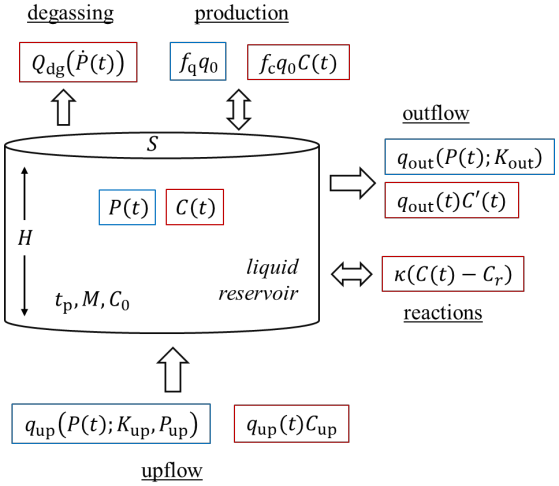

Figure 2: Schematic configuration of lumped parameter model. Blue and red outlined terms refer to liquid and CO_2 transfers, respectively. Symbols are referred to in the text.

The total mass of reservoir fluid is $M = V\rho\phi$ and is assumed to not change significantly with pumping (i.e., it is also held constant where convenient to do so). For typical values (S=10 km^2, H=100 m, ρ=10^3 kg.m^{-3}, ϕ=0.1), M is 10^{11} kg but this could be an order of magnitude higher or lower depending on field characteristics or compartmentalisation.

Mass flows, q [kg.s^{-1}], are subject to Darcy's law and hence proportional to some pressure drop

$$q = -\frac{k\rho A}{\mu}\frac{P - P_{\text{ref}}}{L} \tag{1}$$

where k is permeability [m^2], μ is visocity [Pa.s], A is the area over which flow occurs [m^2], P is hydrodynamic pressure [Pa] defined with respect to a hydrostatic value at the reference depth, P_{ref} is a reference pressure, and L [m] is some characteristic distance across which the pressure drop occurs. It is convenient to use a lumped version of (1)

$$q_i = -K_i(P - P_{\text{ref}}) \tag{2}$$

with K_i [m.s] a reservoir recharge coefficient that collects values of k, ρ, A, μ and L particular to the flow of interest.

Under steady conditions ($dP/dt = 0$), mass flows into and out of the reservoir balance. Defining an upflow that enters the reservoir, and lateral and vertical outflows (to aquifer and through caprock), we can write the mass balance

$$-K_{\text{up}}(P_{\text{up}} - P_0) + K_{\text{aq}}P_0 + K_{\text{cap}}P_0 = 0. \tag{3}$$

Which defines mass rates as negative if entering the reservoir and positive if leaving. In this conceptualization, P_0 is the initial reference pressure, assumed to be higher than hydrostatic, P_{up} is the upflow pressure ($P_{\text{up}} > P_0$) and both outflows are at hydrostatic reference state ($P_{\text{aq}} = P_{\text{cap}} = 0$).

From (3), we can express initial pressure in the reservoir as

Proceedings 47th New Zealand Geothermal Workshop
11 -13 November 2025
Rotorua, New Zealand
ISSN 2703-4275

$$P_0 = \frac{K_{\text{up}}}{K} P_{\text{up}}, \qquad K = \sum_i K_i. \tag{4}$$

where K is a total recharge coefficient for the reservoir. To further simplify, we lump the outflows together as $K_{\text{out}} = K_{\text{cap}} + K_{\text{aq}}$. These can be later disaggregated if it is useful to do so.

2.1 Pressure evolution

We consider a scenario in which the reservoir is extracted from at the constant pumping rate q_0. We allow for reinjection of a fraction of the produced mass back into the reservoir at the rate $(1 - f_{\text{q}})q_0$. Hence, the effective extraction rate is $f_{\text{q}} q_0$ where $f_{\text{q}} = 1$ corresponds to no reinjection and $f_{\text{q}} = 0$ corresponds to full reinjection.

Under net extraction conditions ($f_{\text{q}} > 0$), we expect pressure in the reservoir to drop, and the upflow and outflows to adjust accordingly.

Pressure evolution can be approximated using a lumped parameter model with a linear response term

$$\frac{dP}{dt} = -\underbrace{a_P f_{\text{q}} q_0}_{\text{pumping}} - \underbrace{b_P (P - P_0)}_{\text{linear response}}. \tag{5}$$

For a confined liquid reservoir, pressure changes arise from compressibility of the rock-fluid complex and hence the constants take the form

$$a_P = \frac{1}{\beta_P V \rho \phi}, \qquad b_P = \frac{K}{\beta_P V \rho \phi}, \tag{6}$$

where β_P is the compressibility of water [Pa^{-1}]. For a two-phase boiling model, where pressure changes are reflected in an instantaneously dropping liquid level (instant drainage),

$$a_P = \frac{g}{S\phi}, \qquad b_P = \frac{Kg}{S\phi} \tag{7}$$

where g is the acceleration due to gravity [m.s^{-2}]. Both formulations can be used to approximate K if a_P b_P are known or inferred. Further, b_P has units of [s^{-1}] and is therefore interpreted as the reciprocal of a characteristic time t_{p} that quantifies how rapidly system pressure responds to a perturbation,

$$K = \frac{b_P}{a_P}, \qquad t_{\text{p}} = \frac{1}{b_P} \tag{8}$$

Equation (5) has the solution

$$P = P_0 - \frac{f_{\text{q}} q_0}{K}\left(1 - e^{-t/t_{\text{p}}}\right) \tag{9}$$

which is an exponential decline to a new pressure limit (obtained at $t = \infty$)

$$P_\infty = P_0 - \frac{f_{\text{q}} q_0}{K}, \tag{10}$$

where we have used absolute values to make explicit the pressure drop.

From (10) we observe that higher net extraction leads to larger pressure drops, and this is moderated by the total flow through the system K (Fig. 3).

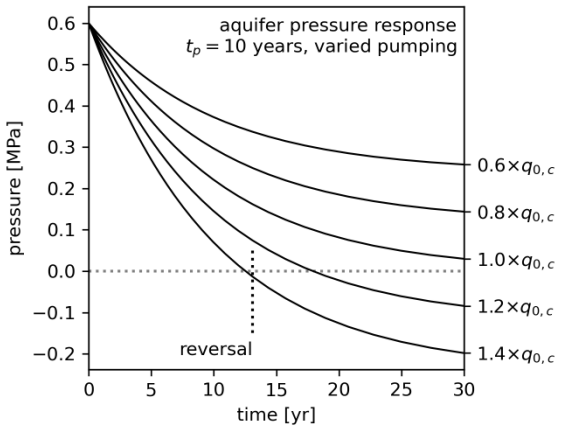

Figure 3: Relative pressure of an aquifer responding to continued pumping. Pumping rates larger than a critical value cause a reversal of the outflow.

2.1.1 Pressure reversal and inflow

Of interest to avoid is the situation that pumping is large enough that it triggers a reversal of the reservoir outflow. This occurs when $P < 0$. The critical pumping rate to trigger a reversal is

$$q_{0,\text{c}} = K P_0 = K_{\text{up}} P_{\text{up}}. \tag{11}$$

For pumping rates exceeding the critical value, the reversal occurs at a time t_{r} given by

$$t_{\text{r}} = t_{\text{p}} \ln\left(\frac{f_{\text{q}} q_0}{f_{\text{q}} q_0 - q_{0,\text{c}}}\right). \tag{12}$$

Reversals are not treated in detail here with attention restricted to situations where $f_{\text{q}} q_0 < q_{0,c}$

2.1.2 Approximation to Wairakei system

Grant and Bixley (2011) suggest typical pressure conditions in geothermal reservoirs about 10% higher than hydrostatic. For a 600 m deep reservoir, hydrostatic pressure is about 60 bar, in which case we would expect P_0 to be approximately 6 bar. This can be achieved by setting P_{up} to 12 bar, assuming $K_{\text{up}} \approx K_{\text{out}}$, which we would typically do in the absence of better information.

Fradkin et al. (1981) describe an improved version of (5) that accounts for non-instantaneous drop of the reservoir liquid level. Applying this model to production data from Wairakei, they inferred a_P = 3.1×10^{-6} m^{-1} s^{-2} and b_P = 3.0×10^{-9} s^{-1}. For these values, we compute t_P as 10 years and K as 10^{-3} m.s.

With these values, we can estimate the reservoir mass throughput under natural state conditions $q_{\text{up}} = -q_{\text{out}} = K_{\text{up}}(P_{\text{up}} - P_0) = 300$ kg.s^{-1}, which is of a similar order to the 400 kg.s^{-1} natural outflow estimated by Allis (1981) for Wairakei.

2.2 Dissolved CO_2 model

Here, we principally deal with CO_2 that is dissolved in the reservoir fluid. CO_2 is characterized by its concentration C [kgCO_2/kgH_2O], defined here as a mass fraction

Proceedings 47th New Zealand Geothermal Workshop
11 -13 November 2025
Rotorua, New Zealand
ISSN 2703-4275

$$C = m_{CO_2}/m_{H_2O}. \quad (13)$$

Under steady (pre-pumping) conditions, CO_2 enters the reservoir via the upflow at a concentration C_0. The reservoir and outflows are at the same concentration.

A mass-balance of CO_2 in the liquid part of the reservoir is

$$M\frac{dC}{dt} = -\underbrace{q_{up}C_{up}}_{\text{upflow}} - \underbrace{f_C q_0 C}_{\text{pump}} - \underbrace{q_{out}C'}_{\text{outflow/ reversal}} - \underbrace{\kappa(C - C_r)}_{\text{chemical reactions}} - \underbrace{Q_{dg}(\dot{P})}_{\text{degas}} \quad (14)$$

This expression approximates the following processes:

1. Changes in upflow or outflow under the evolving pressure regime. If the reservoir is outflowing, then $C' = C$, but this changes to $C' = C_{out}$ if there is a reversal. Flow rates q_{up} and q_{out}, through pressure, are (generally exponential) functions of time, i.e., $q_i\big(P(t)\big)$.

2. Removal of CO_2 from the reservoir via extraction, but allowing that some portion of this CO_2 may be directly returned to the reservoir via reinjection, with the effective removal parameterized by f_C (similar to f_q, a value of $f_C = 1$ corresponds to no reinjection of CO_2 and $f_C = 0$ corresponds to full reinjection of CO_2 into the reservoir). Note, outfield reinjection of CO_2 that results in no reservoir returns should use $f_C = 1$.

3. Chemical reactions that buffer changes in CO_2 away from some other reservoir (e.g., mineral calcite.). The constant κ [kg.s^{-1}] moderates the rate of reaction and may depend on kinetics, surface area or other factors. The term $C_r(t)$ is a second dependent variable with dimensions of concentration that characterizes the buffer. The term $\kappa(C - C_r)$ is a simplified model whereby CO_2 is produced or removed in proportion to the degree of disequilibrium. Here, we consider only infinite reservoirs that seek the initial, hence $C_r = C_0$. An alternative is a strongly CO_2 fixing reservoir, in which case $C_r = 0$.

4. A source term Q_{dg} [kgCO_2 s^{-1}] that tracks the loss of CO_2 mass into a gas phase through pressure driven reduction of its solubility, i.e., degassing. If reservoir storage becomes solubility limited to $C_s(P)$, then upflowing CO_2 will need to be partitioned with $C_{up} = C_s(P)$ entering the reservoir and the balance contributing to steady degassing. For simplicity, we ignore its time dependence and set $C_{up} = C_s(P_\infty) = C_{s,\infty}$.

2.2.1 Saturation effects

The maximum possible concentration of CO_2 in the liquid phase is determined by its solubility C_s. The solubility in turn depends on temperature, and pressure, the latter exercising an approximately linear effect

$$C_s = \left.\frac{dC_s}{dP}\right|_T \big(P - P_{s,ref}\big) + C_{s,ref} \quad (15)$$

where $P_{s,ref}$ = 1.5 MPa, $C_{s,ref}$ = 0.01, linear slope dC_s/dP [wt% MPa^{-1}] is a quadratic function of temperature (see appendix). Equation (15) is correct to about 1% for P between 5 and 15 MPa and T between 150 and 280°C.

Thus, for a liquid reservoir that is CO_2-saturated, i.e., $C = C_s$, depressurization will induce an amount of degassing and CO_2 loss in proportion to the reduction in solubility

$$Q_{dg}(t) = M\left.\frac{dC_s}{dP}\right|_T \frac{dP}{dt} = \frac{f_q q_0 M}{K t_p}\left.\frac{dC_s}{dP}\right|_T e^{-t/t_p} \quad (16)$$

Thus, the degassing rate is exponential and principally controlled by the pumping rate.

2.2.2 Boiling effects

For reservoirs close to the boiling-point-for-depth curve, depressurization may lead to boiling. As the two-phase reservoir boils, it cools and follows the saturation curve, $T_{sat}(P)$. Thus, degassing must account for both temperature and pressure changes as solubility moves along this curve $C_s\big(P, T_{sat}(P)\big)$. The degassing rate becomes:

$$Q = \frac{f_q q_0 \rho g}{H}\underbrace{\left(\left.\frac{\partial C_s}{\partial P} + \frac{\partial C_s}{\partial T}\frac{\partial T_{sat}}{\partial P}\right)\right|_T}_{\substack{\text{derivative along}\\ \text{saturation curve}}} e^{-t/t_p} \quad (17)$$

which is similar to (16) apart from the derivative term. Fortunately, this derivative is approximately constant for pressures less than 11 MPa. The solubility is retrograde above 12 MPa (see Appendix A).

In addition to degassing, CO_2 exits the boiled liquid and comingles with the vapour phase. Boiling and vapour phase evolution are too complex (Grant, 1977; O'Sullivan et al., 1983) for the analytical treatment developed here.

3. RESULTS

3.1 General solution of conservation equation

Time evolution of the mass flows, q_{up} and q_{out} are obtained from the pressure solution

$$q_{up} = -\frac{K_{up}}{K}\Big(P_{up}K_{out} + f_q q_0\big(1 - e^{-t/t_p}\big)\Big) \quad (18)$$

$$q_{out} = \frac{K_{out}}{K}\Big(P_{up}K_{up} - f_q q_0\big(1 - e^{-t/t_p}\big)\Big) \quad (19)$$

Eq. (14) can then be rewritten as

$$\frac{dC}{dt} = \alpha - \beta C - \gamma C e^{-t/t_p} - \delta e^{-t/t_p} \quad (20)$$

where α, β, γ and δ are constants.

$$\begin{aligned}
\alpha &= \frac{C_0}{M}\left(\kappa\frac{C_r}{C_0} + \frac{C_{s,\infty}}{C_0}\frac{K_{up}}{K}\big(P_{up}K_{out} + f_q q_0\big)\right) = \frac{C_0}{t_\alpha}\\
\beta &= \frac{1}{M}\left(f_C q_0 + \kappa + \frac{K_{out}}{K}\big(q_{0,c} - f_q q_0\big)\right) = \frac{1}{t_\beta},\\
\gamma &= \frac{f_q q_0}{M}\frac{K_{out}}{K} = \frac{1}{t_q}\frac{K_{out}}{K}\\
\delta &= \frac{1}{t_q}\left(\frac{K_{up}}{K}C_{s,\infty} + \frac{M}{K t_p}\frac{dC_s}{dP}\right)
\end{aligned} \quad (21)$$

where we have introduced three new time scales for:

1. Loss of CO_2 over time t_β, which is sensitive to the effective CO_2 extraction (f_C), chemical reactions (κ) and outflows (K_{out}).

ISSN 2703-4275

2. Restoration of CO_2 over time t_α, which is sensitive to chemical reactions (κ) and the degassing upflow (K_{out}).

3. A reservoir flushing time t_q that measures how long it takes to replace the reservoir pore fluid mass (M) at the effective extraction rate ($f_\text{q} q_0$).

Note, if the reservoir is not initially saturated and does not reach saturation during depressurisation, then the second term inside the brackets for δ should be dropped.

A solution to (20) is

$$C' = \exp\left(-bt' + ce^{-t'}\right)\left(C_0' e^{-c} + a(c)^b I(t';\, b, c)\right) \qquad (22)$$

where

$$\begin{gathered} I(t;\, b, c) = \int_{ce^{-t}}^{c} s^{-b-1} e^{-s} ds \\ C' = C + \delta/\gamma, \qquad t' = t/t_\text{p} \\ a = (\alpha + \beta\delta/\gamma) t_\text{p}, \qquad b = t_\text{P}/t_\beta, \qquad c = \gamma t_\text{p} \end{gathered} \qquad (23)$$

The integral $I(t;\cdot)$ can be evaluated numerically using gamma functions. However, the solution has an exponential character at late-time, which is approximated as

$$C = \underbrace{C_\infty}_{\substack{\text{new} \\ \text{eq}^\text{m} \\ \text{conc.}}} + \underbrace{\Delta C_\beta e^{-t/t_\beta}}_{\substack{\text{"fast" reservoir} \\ \text{with } CO_2 \\ \text{bottlenecks}}} + \underbrace{\Delta C_\text{P} e^{-t/t_\text{P}}}_{\substack{\text{"slow" reservoir} \\ \text{conc in} \\ \text{quasi eq}^m}} \qquad (24)$$

where we define the system's new steady state C_∞ that trades off CO_2 loss and restoration times, as well as constants ΔC_β and ΔC_P

$$\begin{gathered} C_\infty = C_0 \frac{t_\beta}{t_\alpha} = C_0 \frac{\kappa \frac{C_\text{r}}{C_0} + \frac{C_{\text{s},\infty}}{C_0}\frac{K_\text{up}}{K}\left(P_\text{up} K_\text{out} + f_\text{q} q_0\right)}{\kappa + f_\text{C} q_0 + \frac{K_\text{out}}{K}(q_{0,c} - f_\text{q} q_0)} \\ \Delta C_\beta = C_0' e^{-c} + a(c)^b \int_0^c s^{-b-1} e^{-s} ds \\ \Delta C_\text{P} = -\frac{ac}{b(1-b)} \end{gathered} \qquad (25)$$

This structure shows that the system exponentially approaches its new equilibrium state (Fig. 4).

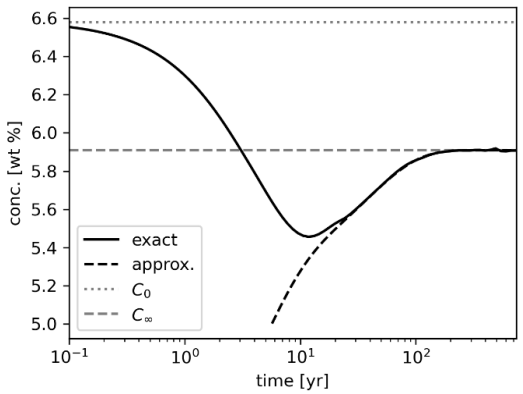

Figure 4: Exact and approximate analytical solutions for reservoir CO_2 concentration showing exponential approach to a new steady state.

In practice, there are two regimes that dominate system behaviour depending on which of the two exponential terms has the larger time constant (the other term more rapidly tends to zero.)

1. If pressure equilibration is rapid (small t_P), then changes in reservoir CO_2 concentration largely reflect CO_2 loss processes (extraction, outflows and chemical equilibria).

2. If pressure decline is slow, reservoir CO_2 content responds quickly and in quasi-equilibrium with contemporary pressure and hydrology.

Once a solution for reservoir concentration has been obtained, individual terms in (14) can be evaluated to compute the changes in reservoir inflow, field and power plant emissions, and mineralisation over time.

3.2 Equilibrium limits

Simple expressions can be derived for the new steady state condition and emissions for several possible limiting cases.

1. *Highly reactive reservoirs.* κ has the largest influence, buffering reservoirs are essentially infinite and therefore $C_\infty = C_\text{r}$ (equilibrium with the rock reservoir). In subsequent cases, we generally restrict our attention to reservoirs where reactivity is small compared to other processes ($\kappa = 0$).

2. *Unequal reinjection rates.* Partial reinjection of the extracted fluid and CO_2 but at unequal proportions, $f_\text{C} \neq f_\text{q}$. The steady CO_2 concentration becomes

$$C_\infty = C_{\text{s},\infty}\left(1 + q_0 K \frac{f_\text{C} - f_\text{q}}{K_\text{out} q_{0,c} + f_\text{q} q_0 K_\text{up}}\right)^{-1} \qquad (26)$$

When fluid and CO_2 injection balance ($f_\text{C} = f_\text{q}$) concentration changes in the reservoir reflect pressure-solubility effects only ($C_{\text{S},\infty}$). In the case of imbalanced reinjection, the reservoir tends to a new equilibrium that is either diluted ($f_\text{q} < f_\text{C}$) or concentrated ($f_\text{q} > f_\text{C}$) compared to the upflow. Note, the latter is only possible in the case of a solubility unconstrained system, in which case the substitution $C_{\text{s},\infty} = C_0$ should be made in (26).

3. *A new emissions equilibrium.* Total CO_2 emissions partition into field and plant components. At the new steady state, the field emissions are

$$Q_{\text{fld},\infty} = \underbrace{\frac{K_\text{out}}{K} P_\text{up} K_\text{up} C_0}_{\substack{\text{original field} \\ \text{emissions}}} + \underbrace{\frac{K_\text{up}}{K} f_\text{q} q_0 C_0}_{\substack{\text{induced} \\ \text{upflow}}} - \underbrace{f_\text{C} q_0 C_\infty}_{\substack{\text{plant} \\ \text{emissions}}} \qquad (27)$$

Thus, emissions from the field are partly increased by increased upflow induced through pressure decline but this is offset by production that diverts some emissions to the plant. Total emissions from the field will always be increased due to the induced upflow effect. This will be absent in models that instead assume a fixed inflow (e.g., O'Sullivan et al., 2021).

3.3 High-gas, solubility-limited fields

Two end-members are worth examining. The first is a high-gas system whose initial concentration of CO_2 in the reservoir is constrained by solubility at relevant pressure and temperature. Examples could include shallow compartments of Ngāwhā or Ohaaki fields, with the latter exhibiting 3wt%

Proceedings 47th New Zealand Geothermal Workshop
11 -13 November 2025
Rotorua, New Zealand
ISSN 2703-4275

CO_2 content at 60 bar in the shallow reservoir (O'Sullivan et al., 1985), close to the expected solubility.

A model of an Ohaaki-like field is shown in Fig. 5, with 60% reinjection of produced fluid and variable rates of CO_2 capture. This field has initial CO_2 content of 3.5wt%, natural state emissions of 33 kt.yr^{-1}, and pressure depletion from 60 to 24 bar. Initial production drives reservoir degassing of up to 18 kt.yr^{-1} (Fig. 5(b)) for the first two decades as the reservoir pressure adjusts to the new equilibrium. A similar response is observed in O'Sullivan et al. (2021) coincident with the start of production. Reservoir concentrations decline (Fig. 5(a)) in response to degassing and reinjection dilution.

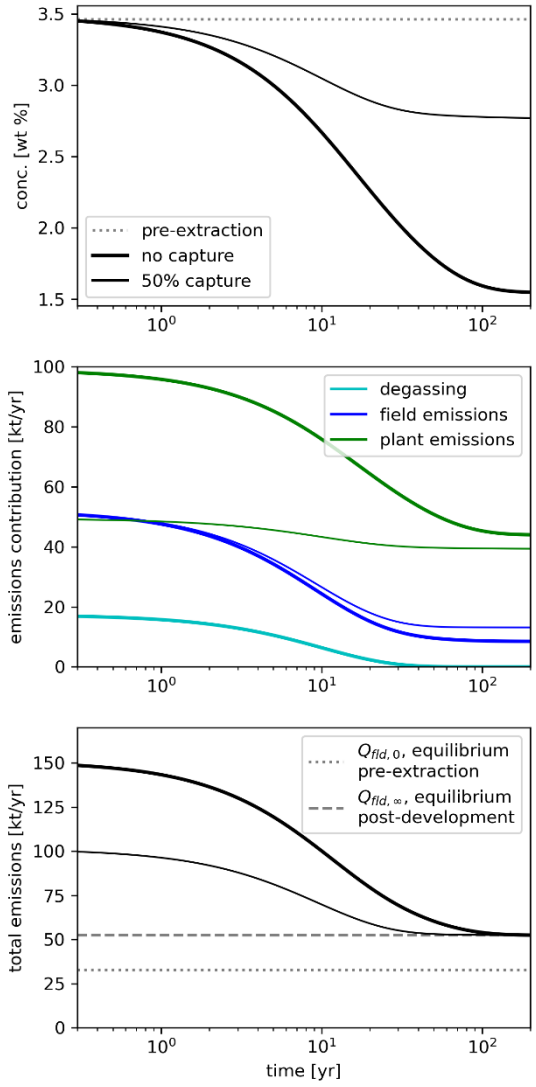

Figure 5: A high-gas, solubility-constrained field with K=10^{-4} m.s, 60% fluid reinjection, and zero (bold) or 50% CO_2 capture (non-bold). (a) Reservoir CO_2 concentration, (b) degas (cyan), field (blue) and plant (green) emissions, and (c) total emissions relative to equilibrium values (grey dashed and dotted lines).

Field emissions are higher than the natural state at early time, primarily due to the degassing, but later drop below the natural state as outflows diminish and reservoir concentration drops (Fig. 5(b)). Plant emissions remain higher than field emissions by a factor of 2 to 5. Total emissions always exceed the old steady state (Fig. 5(c)) and steadily tend towards a new higher equilibrium reflecting the induced upflow.

3.4 Low-gas fields with full capture and mineralisation

The second end-member is a low-gas field where solubility constraints are not immediately relevant (Fig. 6). This field is more Wairakei-like, having a higher mass throughput (K=10^{-3} m.s) but lower initial CO_2 concentration (0.3wt%). We consider the case of 60% fluid reinjection and three CO_2 capture scenarios: no capture, 100% capture, and 110% capture. In the latter, an additional 10% of CO_2 is injected into the reservoir as a negative emissions strategy (e.g., Titus et al., 2025).

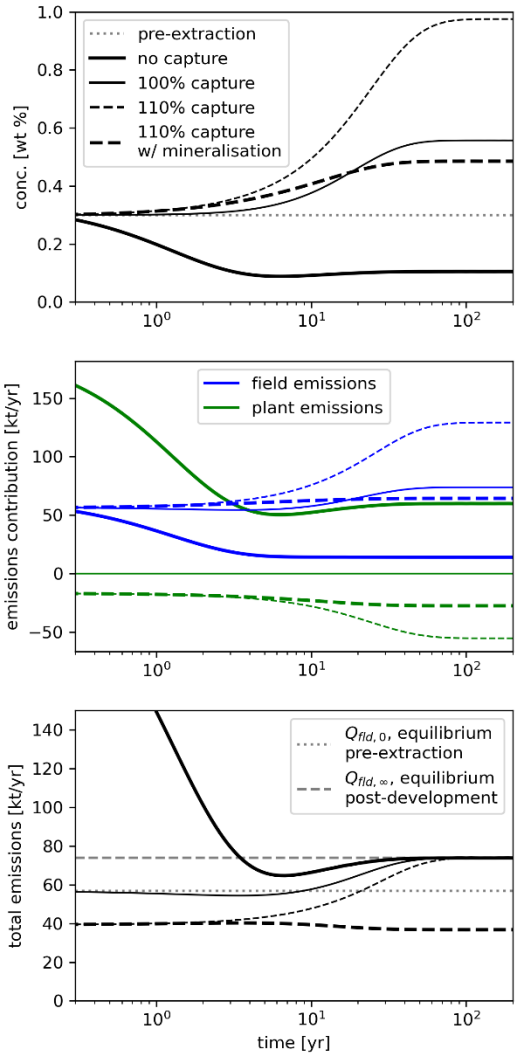

Figure 6: A low-gas field (K=10^{-3} m.s) with no degassing (bold solid) and capture of 100 (solid) or 110% of produced CO_2 (dashed). Mineralisation reactions are also included for one case (bold dashed). (a) Reservoir CO_2 concentration, (b) degas (cyan), field (blue) and plant (green) emissions, and (c) total emissions relative to equilibrium values (grey dashed and dotted lines).

Proceedings 47th New Zealand Geothermal Workshop
11 -13 November 2025
Rotorua, New Zealand
ISSN 2703-4275

The effect of CO_2 capture exceeding reinjection ($f_C > f_q$) is one of a concentrating of CO_2 in the reservoir: an approximate doubling to 0.55wt% for the case of 100% CO2 capture, and about 1.0wt% for the carbon removal case of 110% capture. For the latter scenario, although plant emissions are increasingly negative over time (Fig. 6(b)), the concentrating of CO_2 in the reservoir increases the natural field emissions in equal proportion. The net impact on total emissions is eventually the same for all scenarios (Fig. 6(c)), although the lower capture scenarios had higher emissions at early times. This result highlights the advice of Titus et al. (2025) that if carbon removal is to be undertaken in geothermal systems, particular care must be taken that re-entry of injected CO_2 into the reservoir be minimised as much as possible.

For illustration purposes, we considered the possibility that mineralisation reactions within the reservoir might partially restore elevated CO_2 concentrations back to their equilibrium level. The quite rapid mineralisation that occurs with basalts at CarbFix should use a reaction time constant of M/κ=2 months (Snæbjörnsdóttir et al., 2020). For this example, we used a reaction time constant of 5 years (30-times slower) and assumed $C_r = C_0$, applying this to the negative emissions scenario.

The principal effect of mineralisation reactions is to reduce CO_2 concentration in the reservoir, which stabilises at about half the value it would have reached if no reactions were present (Fig. 6(a)). This in turn reduces the field emissions (Fig. 6(b)) and ensures overall total emissions remain below even the initial natural state for this field (Fig. 6(c)). Mineralisation reactions are clearly a key process for secure, long-term carbon storage in negative emissions scenarios.

4. DISCUSSION AND CONCLUSIONS

Several studies have directly measured the flux of CO_2 from the surface of NZ geothermal systems. Of particular note are two surveys of Rotokawa (Bloomberg et al., 2014; Yang et al. 2024) that reported fluxes from 126 to 161 kt.yr^{-1}. These are somewhat higher than the 20 kt.yr^{-1} from Seward and Kerrick (1996) that relies solely on reservoir composition, and does imply that tank models of the type developed here don't capture a complete picture of field emissions. Nevertheless, repeated CO_2 flux surveys of this kind would be useful to verify some of the behaviours modelled here and elsewhere, including early-time degassing and steady emissions decline (Fig. 4(b), 5(b); Fig. 13 of O'Sullivan et al., 2021).

The current emissions pricing scheme in NZ (the Emissions Trading Scheme – ETS) charges geothermal operators for CO_2 emissions derived from produced geothermal fluids that are subsequently discharged to the atmosphere. While more straightforward to measure, this does not always provide an accurate picture of the impact of production on a field's emissions. For instance, the hypothetical high-gas field in Fig. 5(b) shows plant emissions dropping from ~100 kt.yr^{-1} to ~50 kt.yr^{-1} as the field degases over its lifetime. However, total emissions from the field *in excess* of its pre-development equilibrium range from 130 kt.yr^{-1} to ~20 kt.yr^{-1}. In the early years, emissions charges based on the power plant underestimate total emissions by not accounting for reservoir degassing, while at later time they overestimate by not accounting for the field's reduced outflow.

In a second example, a field with 100% emissions capture and injection would pay no emissions charge (Fig. 5(b)), even though the total emissions through the field had increased post-development (Fig. 5(c)) as a result of induced upflow. These captured emissions do ultimately end up at the surface, at least in these models that conceptualise the system as a flow-through reservoir rather than a static storage container. If nothing else, these simple examples demonstrate that regulatory frameworks appropriate for carbon capture and storage in hydrocarbon fields are not appropriate for the fluxing nature of geothermal systems.

Several improvements to the model developed here are suggested. First, we should include an account of the complex dynamics of gas cap composition, including the preferential concentration of a CO_2 component. Second, the current model assumes that exsolved CO_2 instantly exits the field through a leaky caprock. In practice, there will be a delay associated with gas flux through the near-surface. This could have implications for monitoring the time-varying surface CO_2 flux of a geothermal system. Third, a sufficiently large pressure decline could trigger a reversal of the outflow that brings relative dilute surface waters into the reservoir, further reducing CO_2 concentrations and natural emissions. It is proposed that this be addressed through the C' term in (14).

ACKNOWLEDGEMENTS

This research was supported by MBIE contract UOC2456 "Derisking Carbon Dioxide Removal at Megatonne Scale in Aotearoa" Endeavour Research Program.

REFERENCES

Allis, R. G. (1981). Changes in heat flow associated with exploitation of Wairakei geothermal field, New Zealand. *New Zealand Journal of Geology and Geophysics, 24*(1), 1-19.

Bertani, R., Thain, I. (2002). Geothermal power generating plant CO2 emission survey. IGA news, 49, 1-3.

Bloomberg, S., Werner, C., Rissman, C., Mazot, A., Horton, T., Gravley, D., Kennedy, B., Oze, C. (2014). Soil CO_2 emissions as a proxy for heat and mass flow assessment, Taupō Volcanic Zone, New Zealand. *Geochemistry, Geophysics, Geosystems 15*, 4885-4904.

Duan, Z., Sun, R. (2003). An improved model calculating CO2 solubility in pure water and aqueous NaCl solutions from 273 to 533 K and from 0 to 2000 bar. *Chemical Geology 193* (3-4), 257–271.

Fradkin, L. J., Sorey, M. L., & McNabb, A. (1981). On identification and validation of some geothermal models. *Water Resources Research, 17*(4), 929-936.

Giggenbach, W. F. (1995). Variations in the chemical and isotopic composition of fluids discharged from the Taupo Volcanic Zone, New Zealand. *Journal of Volcanology and Geothermal Res, 68*(1-3), 89-116.

Grant, M. A. (1977). Broadlands—a gas-dominated geothermal field. *Geothermics, 6*(1-2), 9-29.

Grant, M. A., & Bixley, P. F. (2011). Geothermal reservoir engineering. Academic Press.

Kaya, E., & Zarrouk, S. J. (2017). Reinjection of Greenhouse Gases into Geothermal Reservoirs. *International Journal of Greenhouse Gas Control, 67*, 111–129.

McLean, K., Richardson, I., Hanik, F., Siega, F., & Gibson, B. (2024). Reducing greenhouse gas emissions from NZ geothermal power stations. Proceedings *46th New Zealand Geothermal Workshop*, Auckland, NZ.

O'Sullivan, J., Gravatt, M., Riffault, J., Renaud, T., O'Sullivan, M., Ruiz, N. C., ... & Mannington, W. (2025). An updated model of Ohaaki geothermal field, New Zealand. *Geothermics, 130*, 103339.

O'Sullivan, M. J., Bodvarsson, G. S., Pruess, K., & Blakeley, M. R. (1985). Fluid and heat flow in gas-rich geothermal reservoirs. *Society of Petroleum Engineers Journal, 25*(02), 215-226.

O'Sullivan, M., Gravatt, M., Popineau, J., O'Sullivan, J., Mannington, W., & McDowell, J. (2021). Carbon dioxide emissions from geothermal power plants. *Renewable Energy, 175*, 990-1000.

Seward, T. M., & Kerrick, D. M. (1996). Hydrothermal CO2 emission from the Taupo volcanic zone, New Zealand. *Earth & Planetary Science Letters, 139*(1-2), 105-113.

Siahaan, Y., Kaya, E., Altar, D.E., Mering, J., Subekti, D., Utami, A., Atayde, R., Melia, K., & Sepulveda, F. (2024). Reactive Transport Modelling of Fluid-NCG Reinjection in Ngā Tamariki Geothermal Field, *Proc. 46th New Zealand Geothermal Workshop*, Auckland, New Zealand.

Snæbjörnsdóttir, S. Ó., Sigfússon, B., Marieni, C., Goldberg, D., Gislason, S. R., & Oelkers, E. H. (2020). Carbon dioxide storage through mineral carbonation. *Nature Reviews Earth & Environment, 1*(2), 90-102.

Swanepoel, A., Raihannur, M., Karan, A., Gravatt, M., Tonkin, R., O'Sullivan, J., Riffault, J., & O'Sullivan, M. (2024). Investigations of Reservoir Response to Net Negative CO_2 Reinjection using Full Scale Geothermal Reservoir Models, *Proc. 46th New Zealand Geothermal Workshop*, Auckland, New Zealand.

Titus, K., Dempsey, D., Peer, R., & Hanik, F. (2025). From carbon neutral to carbon negative: a theoretical bioenergy and CO2 removal retrofit at Ngāwhā geothermal power station. *Journal of the Royal Society of New Zealand, 55*(4), 893-911.

Yang, T.-H. J., Chamberfort, I., Rowe, M. Mazot, A., et al. (2024). Variability in surface CO2 flux: Implication for monitoring surface emission from geothermal fields. *Geothermics 120*, 102981

APPENDIX

A. Thermodynamic functions

Here, we present approximate expressions for CO_2 solubility and its derivatives, derived from the thermodynamic model of Duan and Sun (2003).

Eq. (15) expresses solubility as a linear function of pressure (Fig. A(a)) with a slope parameter whose temperature dependence is closely approximated by a quadratic expression (Fig. A(b))

$$\left.\frac{dC_s}{dP}\right|_T = \sum_{i=0}^{2} c_i T^i \tag{28}$$

where c_i=[4.5848×10^{-3}, -3.3141×10^{-5}, 1.3104×10^{-7}].

For systems that are boiling, pressure and temperature follow the saturation curve. CO_2 solubility in the pressure range 5 to 15 MPa can be approximated by the following cubic expression accurate to 1.2%

$$C_s(P, T_{sat}(P)) = \sum_{i=0}^{3} c_i P^i \tag{29}$$

where c_i=[6.3416×10^{-2}, -2.1793×10^{-2}, 3.7815×10^{-3}, -1.6108×10^{-4}] (Fig. A(c)). The expression is approximately linear in the pressure range 3 to 11 MPa with the following expression also accurate to 1.2%

$$C_s(P, T_{sat}(P)) = \sum_{i=0}^{1} c_i P^i \tag{30}$$

where c_i=[-6.3404×10^{-3}, 6.8163×10^{-3}].

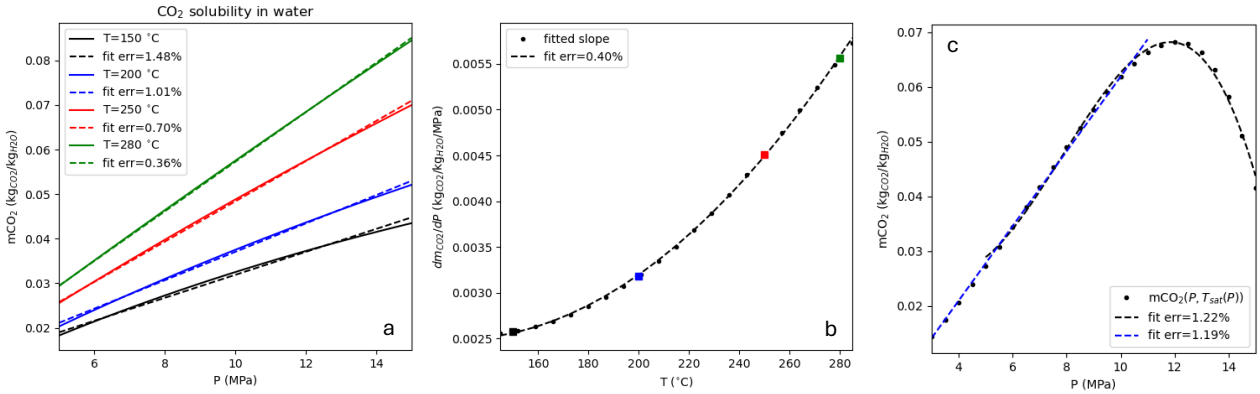

Figure A: CO_2 solubility approximations. (a) Linear approximations in the range 5 to 15 MPa for different temperatures. (b) Linear slope parameter in (a) as a quadratic function of temperature. (c) Linear and cubic approximations to solubility along the boiling curve.